Mixing interfaces, fluxes, residence times and redox conditions of the hyporheic zones induced by dune-like bedforms and ambient groundwater flow

Alessandra Marzadri[a], Daniele Tonina[a], Alberto Bellin[b], Alberto Valli[c]

[a]*Center for Ecohydraulics Research, University of Idaho, Boise, Idaho, USA.*
[b]*Department of Civil, Environmental and Mechanical Engineering, University of Trento, Trento, Italy.*
[c]*Department of Mathematics, University of Trento, Trento, Italy.*

Abstract

Recent studies highlighted the importance of the interface between streams and their surrounding sediment, known as the hyporheic zone, where stream waters flow through the alluvium. These pore water fluxes stem from the interaction among streambed morphology, stream hydraulics and surrounding groundwater flow. We analytically model the hyporheic hydraulics induced by a spatially uniform ambient groundwater flow made of a horizontal, underflow, and a vertical, basal, component, which mimics gaining and losing stream conditions. The proposed analytical solution allows to investigate the control of simple hydromorphological quantities on the extent, residence time and redox conditions of the hyporheic zone, and the thickness of the mixing interface between hyporheic and groundwater cells. Our analysis shows that the location of the mixing zone shallows or deepens in the sediment as a function of bedform geometry, surface hydraulic and groundwater flow. The point of stagnation, where hyporheic flow velocities vanish and where the separation surface passes through, is shallower than or coincides with the deepest point of the hyporheic zone only due to underflow. An increase of the ambient flow causes a reduction of the hyporheic zone volume similarly in both losing and gaining conditions. The hyporheic residence time is log-normally distributed under neutral, losing and gaining conditions, with the residence time moments depending on the same set of parameters describing dune morphology and stream flow.

Key words:

Preprint submitted to Advances in Water Resources *December 11, 2015*

stagnation points, mixing layer, river morphology, hyporheic flows, groundwater

---

1. Introduction

Stream waters downwell into the streambed sediment and then reemerge into the stream at upwelling areas, delineating a subsurface volume in which the sediments are saturated with stream waters [see e.g., 59, 28]. These fluxes are chiefly controlled by the spatial and temporal variations of near-bed energy heads and sediment hydraulic conductivity, but are also influenced by the extension of the alluvial area, turbulence, sediment transport and water density gradients between stream and pore waters [62, 6]. They form the so called hyporheic exchange, which is the primary mechanism bringing oxygen-rich and solute-laden stream waters within the streambed sediments [10, 2, 63, 65]. Similarly, hyporheic exchange brings reduced-element laden waters from the low-oxygen concentration environment of the streambed sediment to the surface water environment [69, 77, 37], thereby creating chemical and physical gradients that sustain an ecotone rich in organisms density and diversity [18]. These fluxes can extend vertically and laterally, depending on stream sinuosity, alluvial sediment stratification and bedrock outcrop [70, 36, 11, 9, 64]. They can be classified as fluvial hyporheic fluxes, which mainly extend vertically within the channel wetted areas, parafluvial fluxes, which flow below dry bars within the active channel, and floodplain fluxes, which include inter-meander fluxes and preferential flow paths along paleochannels [18, 59].

Near-bed pressure distribution due to variations in dynamic head, hydrostatic head or a combination of the two, is recognized as the main mechanism driving hyporheic exchange in natural systems [6, 26, 27, 61, 64]. This distribution depends on the interaction between surface flow and streambed topography [19, 13, 42] at several spatial scales [57, 62, 43, 9]. For small-scale bedforms, such as dune, dynamic head variations generate low pressure zones downstream from the dune crests, where flow detaches, and high pressure zones along dune stosses, where flow reattaches [71, 53, 58].

The hyporheic flow field generated by dune-like morphology received a great deal of attention starting from the analytical solutions proposed by Elliott and Brooks [19] for the hyporheic flow field of an infinite alluvium thickness with only horizontal groundwater flow, called underflow. Their solution was successively extended by Packman et al. [45] for the case of a finite alluvium thickness to study infiltration of colloidal sediments into the streambed by adding the particle settling velocity [e.g., 46, 47, 48]. Marion et al. [36] investigated the effect of stratified sediments on hyporheic exchange. These cases did not consider the vertical component of the groundwater flow referred as basal flow [14], which Boano et al. [7, 8] added to the solution of Elliott and Brooks [19] with the superposition of the effects by taking advantage of the linearity of the Laplace equation. They used the solution, derived for an infinite vertical domain, to investigate the effects of upwelling basal flows on limiting hyporheic zone vertical extension, residence time and mean downwelling flux. They also explored hyporheic exchange variations along a stream cross-section due to the decrease of upwelling basal flows from stream banks to the center. Cardenas and Wilson [14] numerically studied the effect of both upwelling and downwelling basal flows and finite alluvium depth on hyporheic flow induced by large dunes with different aspect ratios (the ratio between dune amplitude and depth, which they defined as steepness). The general trend of their numerical results was confirmed by the recent work of Fox et al. [23], who provided the first experimental support on the effects of groundwater flows on hyporheic zone extension and fluxes. With a numerical model, Hester et al. [31] underlined the importance of the interaction between surface water and groundwater on shaping hyporheic flow streamlines and therefore on the extension of the hyporheic zone. They showed that the separation surface between ground water and hyporheic flow cells delineates the effective volume of sediment where these two waters mix. Werth et al. [72] defined the depth of this surface as a "*dispersion distance*", which can be interpreted as an indirect measure of mixing between the two water systems: hyporheic and groundwater. The separation surface passes through the so called stagnation points where flow velocity has zero magnitude [3]. Jiang et al. [33] argued the importance of the location of those points as a useful index "*to characterize the location of topography-driven groundwater flow in drainage basins*" [67, 73, 33].

All these previous works do not present a comprehensive analysis that quantify and predict hyporheic hydraulics, including the form of the hyporheic residence time distribution, RTD, and its associated moments, i.e. mean, median and variance, and the location of the stagnation points as a function of hydro-morphological parameters measurable in the field. The knowledge of the RTD and its moments is vital information in interpreting hyporheic processes of reactive solutes at the local scale [77, 10, 37] and to upscale them at the reach stream segment scale [30, 41, 25]. Consequently, our objectives are to analyze and quantify hyporheic fluxes, the vertical extent of the hyporheic flow cells, and the associated residence time distribution, together with other relevant quantities such as the hyporheic zone potential redox condition, and the location of the separation surface between hyporheic and ground waters and the thickness of the associated mixing layer as a function of bedform size, stream hydraulics, groundwater flow (underflow and basal flows) and alluvium depth. More specifically we aim to quantify: i) the statistical moments of the RTD; ii) whether the probability density function, pdf, of the RTD remains a lognormal distribution [75] under different forcing conditions; and iii) the effects of gaining and losing conditions on the global biogeochemical status of the hyporheic zone.

To address our objectives, we derived an analytical solution, which we coupled with the Damköhler number concept, for the hyporheic flow field induced by two dimensional dune-like bed-forms with finite alluvium depth and ambient groundwater flow, here represented with spatially uniform horizontal (underflow) and vertical (basal flow) components.

2. Methods

2.1. Analytical solution of the hyporheic flow field

The hyporheic flow field is modeled as a Darcian flow [see e.g., 24]:

$$\mathbf{u} = -\mathbf{K} \cdot \nabla h \tag{1}$$

where $\mathbf{u}$ is the specific discharge, which in agreement with Elliott and Brooks [19] we indicate as[REV] seepage velocity, $\mathbf{K}$ is the hydraulic conductivity tensor and h is the energy head. We assume a homogenous and isotropic hydraulic conductivity tensor and stationary flow conditions, such that the flow governing equation reduces to:

$$\frac{\partial^2 h}{\partial x^2} + \frac{\partial^2 h}{\partial y^2} = 0 \tag{2}$$

Here, along the original works of Elliott and Brooks [19] and Packman et al. [45], we solve analytically the governing equation (2) for hyporheic flow induced by two-dimensional dune-like bedforms in a rectangular domain of length L equal to the dune length and thickness d_b, measured from the average streambed elevation to the underlying horizontal surface, representing the lower impervious boundary. In addition, we consider the following boundary conditions: i) a specified uniform horizontal head gradient, which drives the underflow component of the groundwater flow, equal to the streambed slope, s, ii) a given energy head distribution at $y = 0$ (composed by a periodic part and a linear component), and iii) a specific groundwater vertical seepage velocity, v_{gw}, mimicking the vertical component of groundwater flow normal to the horizontal plane at $y = -d_b$ (see Figures 1a and 1b). These boundary conditions can be written as follows:

$$\begin{cases} h(x,0) = h_m\, cos(\lambda\, x) - s\, x \\ \left.\dfrac{\partial h}{\partial x}\right|_{x\longrightarrow 0} = \left.\dfrac{\partial h}{\partial x}\right|_{x\longrightarrow L} = -s \\ \left.\dfrac{\partial h}{\partial y}\right|_{y\longrightarrow -d_b} = \pm\dfrac{v_{gw}}{K} \end{cases} \tag{3}$$

In the third equation of (3) the sign + is for losing, while the sign - is for gaining conditions, $\lambda = 2\,\pi/L$ is the dune wavenumber, L is the dune wavelength and h_m is the amplitude of the head distribution at the streambed interface, which is given by Shen et al. [55]:

$$h_m = \frac{0.28\, V^2}{2\, g} \begin{cases} (0.34\, Y^*)^{-3/8} & if \;\; Y^{*-1} < 0.34, \\ (0.34\, Y^*)^{-3/2} & if \;\; Y^{*-1} > 0.34. \end{cases} \tag{4}$$

where V is the mean stream velocity, g is the gravitational acceleration, and Y^* is the ratio between the mean flow depth Y_0 and the dune height H_d [59]. Note that in previous papers [e.g., 19, 45, 8], the given energy head distribution at $y = 0$ was given by a sine function, and the boundary conditions at $x = 0$ and $x = L$ impose the vanishing of the energy head. Here, we have preferred to choose a cosine function, with boundary conditions for the x-derivative of the energy head. This corresponds to focus on a single periodicity cell instead of two adjacents half cells. The approximation of the upper surface with a horizontal plane coinciding with the average streambed elevation does not introduce significant perturbations to the velocity field [19, 45]. The solution for the head is given as the superimposition of two components. The first component is the solution of the equation (2) in the absence of groundwater, i.e. for $v_{gw} = s = 0$ in the boundary conditions (3). The second component is simply a first order polynomial, which once substituted into the Darcy's equation (1) leads to the imposed groundwater flow (see the second and third right hand terms of equation (5)):

$$h(x,y) = h_m\, cos(\lambda x)[tanh(\lambda d_b)\, sinh(\lambda y) + cosh(\lambda y)] - s\, x \pm \frac{v_{gw}\, y}{K} \quad (5)$$

where v_{gw} is a positive quantity and here the assigned + and - signs identify losing and gaining conditions, respectively. Notice that, consistently with the linearity of the flow equation (2), in the absence of the vertical groundwater flow component, i.e. for $v_{gw} = 0$, equation (5) reduces to the solution obtained by Packman et al. [45] and for an infinite alluvium, i.e. $d_b \to +\infty$, it coincides with the solution of Boano et al. [8]. With the head given by the equation (5) the horizontal and vertical components of the seepage velocity assume the following expressions

$$u(x,y) = u_0\, sin(\lambda x)[tanh(\lambda d_b)\, sinh(\lambda y) + cosh(\lambda y)] + u_s \quad (6a)$$

$$v(x,y) = -u_0\, cos(\lambda x)[tanh(\lambda d_b)\, cosh(\lambda y) + sinh(\lambda y)] \mp v_{gw} \quad (6b)$$

where the sign - is for losing, while the sign + is for gaining conditions, $u_0 = K\, \lambda\, h_m$ is the maximum seepage velocity component due to bedform morphology in an infinite alluvium depth (i. e. $d_b \to +\infty$) and $u_s = K\, s$ is the underflow seepage velocity due to the stream slope [19, 45]. Inspection of the vertical component of the ambient groundwater velocity at the streambed surface $y = 0$ in equation (6b) reveals that when $v_{gw} > u_m$ the hyporheic flow is suppressed because flow is everywhere upwelling under gaining and downwelling under losing conditions. Note that $u_m = u_0\, tanh(\lambda\, d_b)$ represents the maximum downwelling seepage velocity [45].

Analytical expressions of the mean hyporheic downwelling fluxes can be obtained by integrating the vertical velocity component of the seepage velocity, given by equation (6b) over the entire dune length to obtain:

$$\begin{cases} \overline{q}_{H,G} = \dfrac{1}{L}\displaystyle\int_{-x_1}^{x_1} [u_m cos(\lambda x) - v_{gw}]dx = \dfrac{u_m}{\pi}\sqrt{1 - \dfrac{v_{gw}^2}{u_m^2}} - \dfrac{v_{gw}}{\pi} arccos\left(\dfrac{v_{gw}}{u_m}\right) \\ \overline{q}_{H,L} = \dfrac{1}{L}\displaystyle\int_{-x_2}^{x_2} [u_m cos(\lambda x) + v_{gw}]dx = \dfrac{u_m}{\pi}\sqrt{1 - \dfrac{v_{gw}^2}{u_m^2}} - \dfrac{v_{gw}}{\pi} arccos\left(\dfrac{v_{gw}}{u_m}\right) + v_{gw} \end{cases} \quad (7)$$

for gaining and losing conditions, respectively. The extremes of integration, x_1 and x_2, in the equations (7) are the smaller horizontal coordinates where

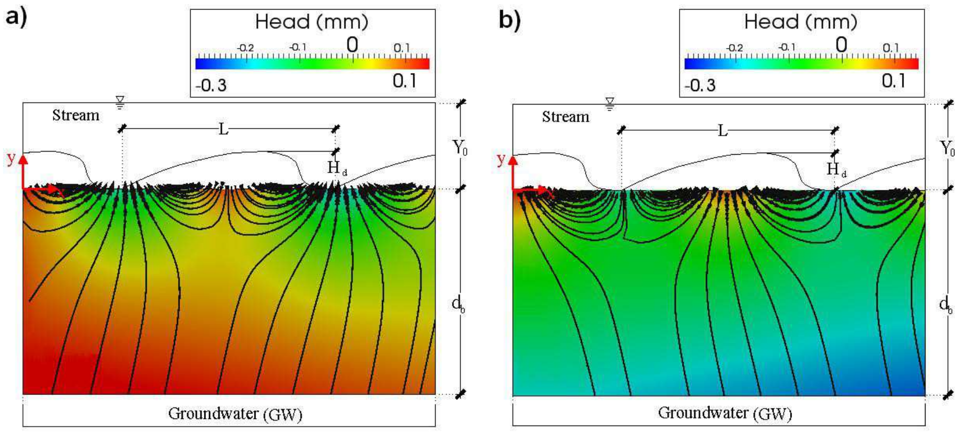

Figure 1: Sketches of 2D dune morphology with groundwater intrusion during (a) gaining and (b) losing conditions. The color map represent the head distribution for the morphology of Test1 in Table S1 (Supplementary Information) when the groundwater velocity is $v_{gw} = \pm 4.3 \times 10^{-7}\, m\, s^{-1}$.

the vertical component of the seepage velocity is zero at the alluvium surface ($v(x, 0) = 0$) under gaining and losing conditions, respectively. Note that $x_1 \in (0, L/4)$; while $x_2 \in (L/4, L/2)$. Equation (7) reduces to the solutions proposed by Packman et al. [45] and by Boano et al. [8] in the case of neutral condition, $v_{gw} = 0$, and of infinite alluvium thickness, $d_b \to +\infty$, respectively. It is also in agreement with the experimental results of Fox et al. [23] because it is able to fit the data reported in their Figure 4 similarly to their model, which is that of Boano et al. [8], in which their sediment thickness ($d_b = 15cm$) is comparable to their dune length ($L = 12cm$) and $d_b \approx L$.

2.2. Delineation of hyporheic zone: stagnation points and separation surface

Previous studies have highlighted that the interaction between stream flow and bedforms and groundwater flows control the formation of hyporheic flow cells [19, 8, 14, 62, 31]. The surface, which separates the hyporheic flow cells from groundwater, can be traced starting from the points where hyporheic and groundwater trajectories diverge [3] and the seepage velocity vanishes. Because of this characteristic, they are called stagnation points [15]. The identification of the stagnation points, which in Figure 2 are at the intersection between gray and black lines, can be done analytically by searching the points where the velocity vanishes. Results show that the stagnation points are characterized by the same depth, y_s for both gaining and losing conditions but by different horizontal locations, which we indicate with x_g and x_l, respectively:

$$\begin{cases} y_s = \dfrac{1}{2\,\lambda} ln\left(\dfrac{u_s^2 + v_{gw}^2 + C_1 + \sqrt{(u_s^2 + v_{gw}^2 + C_1)^2 - u_0^4\,[1 - tanh^2(\lambda\, d_b)]^2}}{u_0^2\,[1 + tanh(\lambda\, d_b)]^2}\right) \\ x_g = \dfrac{1}{\lambda}\left[- arctan\left(\dfrac{u_s\,[tanh(\lambda d_b)\, cosh(\lambda y_s) + sinh(\lambda y_s)]}{v_{gw}\,[tanh(\lambda d_b)\, sinh(\lambda y_s) + cosh(\lambda y_s)]}\right) + 2\pi\right] \\ x_l = \dfrac{1}{\lambda}\left[arctan\left(\dfrac{u_s[tanh(\lambda d_b)\, cosh(\lambda y_s) + sinh(\lambda y_s)]}{v_{gw}\,[tanh(\lambda d_b)\, sinh(\lambda y_s) + cosh(\lambda y_s)]}\right) + \pi\right] \end{cases} \tag{8}$$

where

$$C_1 = \sqrt{\{u_s^2 + v_{gw}^2 + u_0^2\,[1 - tanh^2(\lambda\, d_b)]\}^2 - 4\, u_s^2\, u_0^2\,[1 - tanh^2(\lambda\, d_b)]} \tag{9}$$

Equations (8) identify the stagnation points situated in the region of interest within the flow domain, which is bounded between the streambed interface at $y = 0$ and the bottom of the domain at $y = -d_b$ ($-d_b < y < 0$), provided that the data satisfy the following equation:

$$u_s^2 + v_{gw}^2 + C_1 + \sqrt{[u_s^2 + v_{gw}^2 + C_1]^2 - \; u_0^4\,[1 - tanh^2(\lambda\, d_b)]^2} \leq [u_0^2(1 + tanh(\lambda\, d_b))^2] \tag{10}$$

(Otherwise y_s falls out of the flow domain, as y_s would be > 0). Equations (8) show that the longitudinal coordinates of the stagnation points for gaining and losing conditions are shifted by a value close to $L/2$ in accordance with the shift in the flow field (c.f., Figures 2b and c). Under both gaining and losing conditions, the location of the stagnation points depends on both basal (v_{gw}) and underflow (u_s) flows, on dune size (L), alluvium depth (d_b) and on stream hydrodynamics (through u_0); these are quantities measurable in the field. For completeness, we show, in the Supplementary Information, how equations (8) reduce when specialized to the following three cases: both basal and underflow flows are negligible (i.e., $v_{gw} = u_s = 0$, see equation (S1) in the Supplementary Information), only basal flow is negligible (i.e., $v_{gw} = 0$ but $u_s > 0$, see equation (S3) and (S4) in the Supplementary Information) and only underflow is negligible (i.e., $u_s = 0$ but $v_{gw} > 0$, see equation (S6) in the Supplementary Information).

Winter and Pfannkuch [74] showed that flow systems originate and meet at stagnation points and that the streamlines around these points separate flow systems [44]. The surface separating hyporheic and ground waters is identified by the streamline passing through the stagnation points in the vertical plane. The general expression of a streamline in a planar and divergence-free flow field is the following [[3], ch. 5]:

$$\psi(x, y) = \int [u(x', y')\, dy' - v(x', y')\, dx'] \tag{11}$$

where ψ is the value of the stream function at a given point (x,y), and the integral is taken along the streamline passing thought it. In our case, the extremes of integration are between two adjacent stagnation points, where the streamline starts and ends and (x,y) coincides with one of them (see Figures 2 and 3). Consequently, the streamline separating the two zones is obtained by substituting $\psi(x, y)$ with $\psi(x_g, y_s)$ and $\psi(x_l, y_s)$ into equation (11), which lead to the following algebraic expressions:

$$K\, h_m\, sin(\lambda x)[tanh(\lambda d_b)\, cosh(\lambda y) + sinh(\lambda y)] - v_{gw} x + u_s\, y = \psi(x_g, y_s) \tag{12}$$

and

$$K\, h_m\, sin(\lambda\, x)[tanh(\lambda d_b)\, cosh(\lambda y) + sinh(\lambda y)] + v_{gw} x + u_s\, y = \psi(x_l, y_s) \tag{13}$$

for gaining and losing conditions, respectively which, once solved, provide the loci, i.e. the collection of points (x,y), defining the streamlines in gaining and losing conditions, respectively [see e.g., 32]. For the neutral condition, $x_g = x_l$ and the stream function can be estimated by either equations.

Hyporheic and ground waters can mix along this separation surface [31]. This forms a mixing layer whose thickness, δ_{mix}, can be quantified with the following equation [72]:

$$\delta_{mix} = \sqrt{2\, D_t\, t_{HZ,Lmax}} \tag{14}$$

where $t_{HZ,Lmax}$ is the residence time along the longest streamline within the hyporheic flow cells, which we used in lieu of the separation line whose residence time would be infinite as velocity at the stagnation point is 0. In addition, D_t is the transverse dispersion coefficient evaluated as [4]:

$$D_t = \phi\, D_m + \alpha_t\, \overline{u}_{HZ,Lmax} \tag{15}$$

where D_m is the molecular diffusion coefficient, $\overline{u}_{HZ,Lmax}$ is the mean velocity along this streamline, and α_t is the transverse dispersivity. Note that $D_m = 10^{-9}\, m^2 s^{-1}$ and $\alpha_t = 0.0001m$ [24].

2.3. Characterization of global biogeochemical status of the hyporheic zone

Once the flow field is known and the hyporheic zone delineated, the transport equation is solved along the streamlines connecting downwelling with upwelling areas by means of particle tracking [e.g., 52, 60]. We computed the probability density function (*pdf*) of the residence time distribution by releasing NP particles uniformly distributed within the downwelling area and tracking them up to the upwelling area. Note that in losing conditions particles that exit through the base of the domain are not considered and similarly groundwater particles entering the domain from below for gaining conditions. NP ranges between 500 and 15000 depending on bedform size. In all cases, NP has been chosen to ensure stability of the calculated moments, i.e. no significant changes in the moment values have been observed by increasing the number of particles. The *pdf* is obtained by injecting the NP particle uniformly over the streambed and weighting their residence times by their local fluxes. Consequently, our residence time and residence time moments are all weighted residence time by the downwelling fluxes.

In the present work, we assess the global biogeochemical status of the hyporheic zone through the biogeochemical Damköhler number [38]:

$$Da_O = \frac{\tau_{50}}{\tau_{lim}} \tag{16}$$

where τ_{50} is the median residence time of particles within the alluvium and τ_{lim} is the characteristic time of the biogeochemical reaction, which for the inorganic nitrogen can be estimated as the time needed to consume dissolved oxygen to a concentration at which denitrification occurs. The value of τ_{50} is computed by particle tracking, while τ_{lim} assumes the following form:

$$\tau_{lim} = \frac{1}{K_{RN}} ln\left(\frac{DO_0}{DO_{lim}}\right) \tag{17}$$

where K_{RN} ($K_{RN} = K_R + K_N$) is the reaction rate that combines the effects of nitrification (K_N) and biomass respiration (K_R), which represent the main pathways leading to oxygen consumption within the hyporheic zone [5, 1]. Furthermore, DO_0 is the dissolved oxygen concentration within the stream and DO_{lim} is a threshold concentration below which environmental conditions are classified as anaerobic [38]. In the simulations, we assumed $DO_{lim} = 2\,mg\,l^{-1}$, which is the typical limit value for anoxic condition [49]. In addition, we set $K_R = 0.053\,d^{-1}$ and $K_N = 1.998\,d^{-1}$ obtained applying the Arrhenius equation [22] on the data reported in the works of Rutherford [51] and Sjodin et al. [56], respectively, during a typical winter condition ($T = 6°C$). Through Da_O, we quantify the redox conditions within the streambed sediment. Values of $Da_O > 1$ indicate prevailing anaerobic conditions, whereas values of $Da_O < 1$ indicate prevailing aerobic conditions, within the hyporheic sediment. This metric quantifies the efficiency of the hyporheic zone in transforming dissolved inorganic nitrogen species such as ammonium and nitrate, whose transformation depends on the redox conditions of the hyporheic zone [37, 38]. A similar metric can be estimated for the hyporheic thermal regime [40, 39]. Stream's alluvium is by its nature heterogeneous in both the hydraulic and biogeochemical properties, and this heterogeneity may influence transport and reaction rates of reactive nitrogen, as observed by Sawyer [54] for denitrification at the core scale. However, assessing the effect of heterogeneity analytically is a formidable task in case of non-uniform mean velocity field, while using simulations is impractical at stream and larger scales, as recently discussed by Sawyer [54]. Moreover, as showed in the stochastic groundwater literature [17, 50][REV], the solution of the flow field[REV] for a homogeneous formation is the zero-order solution for a stochastic problem for weakly heterogeneous formations such as those composed by sand and silt, the type of depositional environment in which dunes typically develop.

2.4. Simulations

We consider a wide range of two-dimensional dune-like bedform dimensions to characterize the role of bedform size (bedform amplitude and wavelength), surface hydraulics (mean flow velocity and mean water depth), underflow and basal flows on the hyporheic flow field (see Tables S1-S6 in the Supplementary Information). Bedform dimensions range from small ripple size (wavelength of 10 cm and amplitude of half centimeter) to large dune size (wavelength of 3 m and amplitude of 12 cm). Their hydromorphological characteristics are typical of those found in natural streams [76]. We consider six values of the dune steepness $H_d/L = 0.02, 0.025, 0.03, 0.04, 0.05$ and 0.06, a value of stream slope $s = 0.01\%$ and of 0.04% and 0.14% for few cases, while to keep a reasonable number of simulations without losing generality the remaining parameters are assumed constant: Manning's coefficient is set to $n = 0.0125$ and mean grain size to $d_{50} = 5\,mm$. We set the location where basal velocity is defined at $d_b = L$. The location of d_b defines the alluvium depth in the neutral case.

The characteristic hydraulic parameters of the streamflow can be obtained through the following expressions [34]:

$$Y_0 = \left(\frac{H_d}{\varsigma d_{50}^{0.3}} \right)^{\frac{1}{0.7}} \tag{18}$$

in which ς is the dune height coefficient for which we assume a value between 0.12 and 1. While according to the Manning's equation [21]

$$V = \frac{Y_0^{\frac{2}{3}}\, s^{\frac{1}{2}}}{n} \tag{19}$$

Under these conditions, dune morphology is in equilibrium with the stream flow hydraulics.

The results of the simulations are presented in terms of two new dimensionless numbers, defined as follows:

$$\begin{cases} h_b^* = \dfrac{h_m}{Y_0} \left(\dfrac{L}{H_d} \right)^{0.834} \\ s^* = \dfrac{L\, s}{h_m} \end{cases} \tag{20}$$

where the dimensionless head h_b^* accounts for the effect of both bedform shape and stream hydraulics, through the ratio h_m/Y_0, whereas s^* measures the reciprocal strength of groundwater underflow and bedform induced hyporheic flow. The former is best suited for interpreting the variations of both the thickness of the mixing layer (δ_{mix}) and the Damköhler number, because it scales both the morphological and biogeochemical time scales, τ_{50} and τ_{lim} in a single dimensionless parameter, regardless of dune aspect ratio, H_d/L. On the other hand, s^* is used in combination with dimensionless hydraulic quantities of the hyporheic zone, like the dimensionless hyporheic residence time moments (τ_m^*, τ_{50}^* and σ^{2*}) and the mean dimensionless hyporheic flux ($\overline{q}_{H,i}^*$ with $i = G$ and $i = L$ under gaining and losing conditions, respectively), because it captures the effect of groundwater underflow. We used two dimensionless scales because the dune aspect ratio, which is used for normalizing the hydraulics quantities does not enter in the definition of Da_O. Consequently, to generalize our results on the redox conditions of the hyporheic zone, we account for dune shape by representing Da_O as a function of the dimensionless head h_b^*. The exponent 0.834 (approximate 5/6) was set to collapse all the Da_O numbers along the same trend.

3. Results and Discussion

3.1. Influence of the groundwater on hyporheic zone delineation

The analytical solution of the separation surface, equation (11), allows characterizing the shape of the hyporheic zone starting from hydro-morphologic parameters measurable in the field (Figure 2). The analytical solutions support the numerical results of Cardenas and Wilson [12] for gaining and losing conditions.

In the neutral case, i.e. in the absence of basal flow (v_{gw}=0), the vertical ambient groundwater velocity vanishes at $y = -d_b$, as an effect of the impervious boundary condition. A separation surface, whose shape is influenced by the underflow velocity u_s, develops between surface and subsurface waters (black solid line in Figure 2a) as observed in other works [e.g., 45, 20]. All downwelling particles upwell in the stream and the groundwater flow does not directly enter the stream flow. Thus the hyporheic zone separates the stream from the groundwater flow. In gaining conditions, groundwater upwells and enters into contact with the hyporheic water at the interface between two conterminous hyporheic cells (Figure 2b) [7, 12, 23]. In agreement with other works [15, 23] hyporheic flow cells force the groundwater flow to converge toward the upwelling areas, while downwelling flow separates into two components, one directed upstream and the other downstream, both discharging into the stream in low-head upwelling areas, thereby creating two coupled hyporheic cells. Conversely, in losing conditions, part of stream water downwells almost vertically and mixes with groundwater (Figure 2c) [12, 23]. The remaining part reemerges in upwelling areas. Thus, in gaining conditions all downwelling waters upwell, whereas in losing conditions only a portion of the downwelling waters upwells to the stream. In the latter scenario, physico-chemical properties of the upwelling waters depend on mixing between hyporheic and ground waters.

The streamline that identifies the separation surface between stream and ground waters is indicated by the black solid line in Figure 2, while the gray lines, which are also solutions of equations (12) and (13) indicate the separation surfaces between pairs of hyporheic cells: one upwelling upstream and the other downstream the downwelling area. The cell upwelling upstream is smaller than the cell upwelling downstream, due to the groundwater underflow. The difference in size between the coupled cells grows with underflow intensity (Figure 3a) and the point of stagnation shallows near the streambed interface, as shown by the solid circles in Figure 3a. The upstream-flux cell is suppressed when the underflow energy slope assumes the threshold value of $s = s_{lim} = h_m\lambda$, regardless the basal flow. At this slope, the stagnation point is located at the streambed interface as shown by the green solid circle in Figures 3a and 3b for neutral and losing/gaining conditions, respectively. The separation zone also shallows and its length shortens with consequences on mixing between hyporheic and ground waters [31]. Although the size of the hyporheic cell changes with the streambed slope, s, the separation surface remains symmetric under neutral conditions. It is the basal flow that generates the asymmetric shape of the hyporheic cells under gaining and losing conditions, whose separation surfaces are mirrored once respect to the other and shifted of $L/2$ with respect to the neutral condition. Gaining and losing conditions further shallow the hyporheic zone and shorten the separation surface with respect to the neutral case (c.f., Figures 3b and 3a).

In all analyzed scenarios, we observe a first interface between hyporheic and groundwater flows, represented in Figure 2 with a black line and a second interface between pairs of hyporheic flow cells, represented with a gray line. Location and size of the former interfacial surface is important to quantify mixing and exchange of waters between hyporheic and groundwater domains [72, 31]. These two domains exchange solute with a mass flux that is given by the product of the local dispersion and the gradient of the concentration across the interface. Exchange of heat occurs as well, with the heat flux given by the product of the heat diffusion coefficient and the gradient of temperature across the interface [16]. The hyporheic cells provide a geometrical interpretation of the ecological definition of the hyporheic zone as the volume of sediments saturated with stream water. As suggested by Hester et al. [31], this observation redefines our understanding of the hyporheic zone and, in contrast with the assumptions underlying the Transient Storage Model, it relegates mixing of surface subsurface waters within a portion of the hyporheic volume.

The thickness of the mixing layer, δ_{mix}, given by equation (14) depends on the dimensionless head, h_b^*, and the dimensionless basal flow, $v_{gw}^* = v_{gw}/u_m$, as shown in Figures 4a and 4b. Its thickness increases with dune size, regardless of basal flow scenarios because of the increase of residence time with h_b^*. When the basal flow increases (compare the scenarios in which $v_{gw}^* = 0.1$ with those with $v_{gw}^* = 0.4$ in Figures 4a and 4b), the dimension of the hyporheic flow cell decreases and consequently the longest streamline shortens with a reduction in the mixing layer thickness.

All these behaviors are well fitted by the following three power law functions:

$$\begin{cases} \delta_{mix} = 4.94\,(h_b^*)^{1.30}, \;\; (R^2 = 0.75) \quad \text{for} \;\; v_{gw}^* = 0 \\ \delta_{mix} = 5.36\,(h_b^*)^{1.51}, \;\; (R^2 = 0.90) \quad \text{for} \;\; v_{gw}^* = 0.1 \\ \delta_{mix} = 5.30\,(h_b^*)^{1.67}, \;\; (R^2 = 0.97) \quad \text{for} \;\; v_{gw}^* = 0.4 \end{cases} \tag{21}$$

These regression curves are represented with dashed lines in Figure 4a. The thickness of the mixing layer can be represented also as a function of v_{gw}^*, as shown in Figure 4b. With this parametrization all cases collapse around the following power law expression:

$$\delta_{mix} = 0.0114\,(v_{gw}^*)^{-0.42}, \tag{22}$$

which in Figure 4b is shown with the dashed black line. The high coefficient of determination ($R^2 = 0.98$) suggests that this curve explains with high accuracy the variability of the mixing layer thickness over a wide range of basal flows. Moreover, both gaining and losing conditions tend to the same neutral case value of $\delta_{mix} = 0.187$ when $v_{gw}^* = 0$ and $\delta_{mix} = 0$ when $v_{gw}^* = 1$. This result suggests that the mixing zone is thicker with neutral case and get thinner as ambient groundwater velocity increases. These solutions allow us to predict, from few hydromorphological information, where mixing between water systems occurs and where hyporheic zone provide buffering between surface and subsurface waters.

3.2. Stagnation and deepest hyporheic points

Both Figures 2 and 3 show that the maximum depth reached by the hyporheic cells does not coincide with the stagnation point, which is at a shallower depth. This difference reduces when the ratio $s^* = sL/h_m$ between the head gradient s generating underflow and the averaged hyporheic gradient h_m/L reduces as well, or when basal flow increases. This is illustrated in Figure 5a, which shows the locations of both the stagnation point, y_s^* and the maximum depth of the hyporheic cells, $y_{HZ,min}^*$ as a function of s^*. Both quantities are dimensionless with respect to d_b. Under neutral conditions, even small underflows have a marked effect on both y_s^* and $y_{HZ,min}^*$. Neglecting underflow may lead to an overestimation of y_s^* by as much as 33% and a difference between y_s^* and $y_{HZ,min}^*$ of 20% (see Figures 5a and 5b).

The difference between y_s^* and $y_{HZ,min}^*$ is controlled by the underflow component of the ambient groundwater flow, and it is insensitive to the basal flow, which however modulates the magnitude of the effect of the underflow. Figure 5a shows that a larger basal flow leads to smaller differences between y_s^* and $y_{HZ,min}^*$, but this is limited to small to moderate basal flows. The positions of both y_s^* and $y_{HZ,min}^*$ become insensitive to s^*, and therefore to the strength of underflow $v_{gw} > 0.4u_m$. This is more clearly evidenced in Figure 5b, which shows y_s^* as a function of v_{gw}^*. As expected the stagnation point becomes progressively shallower as the basal velocity increases, with a stronger variation in the range of small values of s^*. However, the effect of s^* weakens as the basal velocity increases, becoming negligible for $v_{gw}^* > 0.9$, when the stagnation point is very close to the stream bed surface.

The minimum value of v_{gw}^* needed to obtain $y_s^* = 0$, which means that the stagnation point is at the stream bed surface, is a function of stream hydromorphology (e.g., dune size and stream flow) and underflow through the value assumed by the energy slope s^* (Figure 5b). While for small to moderate underflow ($s < s_{lim}$) the stagnation point reaches the surface for $v_{gw} \geq u_m$, large underflows, epitomized here with the condition $s > s_{lim}$, reduces the values of v_{gw} at which the stagnation point is located at the surface (Figure 5b).

These results explain and generalize both the experimental [23] and the numerical [14] findings previously obtained and provides an analytical framework for hyporheic zone delineation under the competitive interaction between stream and groundwater. Therefore, they can be used to upscale local processes at the reach or segment scale [25, 41]. In particular, Cardenas and Wilson [14] explained the attenuation of the hyporheic flow cells penetration with the influence of the bedform Reynolds number $Re = V\,H_d/\nu$, where ν is the kinematic viscosity (they used the bedform amplitude as length scale), on the pressure gradients for a constant basal flow. Increasing Re in their simulations was indeed equivalent to increasing dynamic head variations, which are captured in our simulation by h_m. Similarly, our results show that as s^* increases the hyporheic zone becomes shallower. This is in agreement with recent findings of Fox et al. [23], who showed that the value of the basal flow at which the hyporheic flow is suppressed (in their work they called this quantity "q_H") is a result of the competitive interaction between the flow in the stream and the magnitude of the losing/gaining term.

3.3. Hyporheic fluxes

In a recent flume experiment, Fox et al. [23] showed that stream water downwelling flux is the smallest under gaining conditions, intermediate under neutral conditions, and the largest under losing conditions. This behavior, captured by our model through equation (7), is due to the different role that basal flow plays under gaining and losing conditions: additive and of opposite direction, respectively. Similar is the effect of s^* in reducing the mean downwelling flow under both gaining and losing conditions. As s^* increases, the underflow velocity becomes larger relative to the hyporheic flux resulting in a thinner hyporheic cell (see Figure 5), which leads to a reduced downwelling flow (Figure 6a). However, this dependence vanishes when the global hyporheic flux is made dimensionless with respect to u_m (Figure 6b), because the effect of s on h_m is captured by u_m, which varies linearly with respect to s^* as can be shown by equations (4) and (19). Streambed slope affects both underflow and surface hydraulics and thus the near-bed pressure distribution.

3.4. Influence of groundwater flow on the residence time distribution

Here, we use our analytical solution to analyze the effect of the groundwater flow on the hyporheic residence time distribution computed by particle tracking. The hyporheic residence time reduces with increasing v_{gw} as shown in Figures 7a (Test 95 in Table S4 of the Supplementary Information), 7c (Test 105 in Table S4) and 7e (Test 115 in Table S4). The reduction increases with increasing basal flow regardless of gaining and losing conditions, as a consequence of the progressive shrinking of the hyporheic flow cells.

Figures 7b (Test 95 in Table S4), 7d (Test 105 in Table S4) and 7f (Test 115 in Table S3) show the comparison between the sample CDF, of the residence time τ and the log-normal CDF:

$$\bar{R} = 1 - CDF = 1 - \frac{1}{\sqrt{2\pi\sigma_z^2}} \int_0^\tau \frac{e^{-\frac{(ln(\tau') - \mu_z)^2}{2\sigma_z^2}}}{\tau'} d\tau' \tag{23}$$

where μ_z and σ_z^2 are the mean and the variance of the $\log_e$-transformed residence time $z = ln(\tau)$, respectively:

$$\begin{cases} \mu_z = ln\left[\dfrac{\tau_m}{\sqrt{1 + \sigma^2/\tau_m^2}}\right] \\ \sigma_z^2 = ln\left[1 + \dfrac{\sigma^2}{\tau_m^2}\right] \end{cases} \tag{24}$$

with τ_m being the mean and σ^2 the variance of the sample of residence times obtained numerically by particle tracking. The sample's size is equal to the number of particles NP needed to stabilize these two moments, as reported in Section 2.3.

These figures show that the log-normal distribution provides a good match of the sample CDF obtained by numerical simulations under both gaining and losing conditions as already observed for the neutral case in other studies: such as that of Wörman et al. [75] for dunes and of Tonina et al. [66], Marzadri et al. [42] and Trauth et al. [68] for pool-riffle bed forms. This is an interesting result because it allows defining the entire residence time distribution from information on the first two moments of the residence time, which under stationary flow conditions coincide with the moments of the Breakthrough Curve of a non-reactive tracer.

The dimensionless mean and variance depend on s^* for the neutral case. As shown in Figure 8a, the mean dimensionless residence time decreases from 25 for $s^* = 0.02$ to 16 for $s^* = 0.34$. This behavior is due to the underflow velocity that causes the hyporheic flow cells to become asymmetric. As the underflow increases, the upstream-flux cell gets smaller than the downstream-flux cell and the residence times become shorter. Eventually, the upstream-flux cell disappears and the effect on the residence time of the underflow becomes less important as shown in Figure 8a for $s^* > 0.3$. In addition, for $v_{gw}^* \geq 0.1$ the mean residence time τ_m^* assumes a constant value, which depends on the magnitude of the basal groundwater velocity, regardless of s^* for both losing and gaining conditions. As expected, the neutral case results in the largest τ_m^* with an asymptotic limit for large s^*, while τ_m^* is constant with s^* in the presence of basal flows and reduces with increasing v_{gw}^*. This reduction is due to the shallowing and thinning of the hyporheic zone with increasing v_{gw}^*.

Similarly to the mean, for $v_{gw}^* \geq 0.1$ the variance of the dimensionless hyporheic residence time assumes the same constant value for both gaining and losing conditions and its value depends on the basal flow (Figure 8b). Also, the variance is the largest in the neutral case and decreases with increasing s^*. The effect of v_{gw}^* is strong on the residence time variance, which reduces of almost one order of magnitude from the neutral case for $v_{gw}^* = 0.1$ and of 2 orders of magnitude for $v_{gw}^* = 0.4$ (notice the logarithmic scale of the vertical axis). This implies that the residence time distribution sharpens considerably with increasing v_{gw}^* for both the losing and gaining cases, while it is insensitive to s^*. In the neutral case, however, the variance reduces as s^* increases, thereby sharpening the residence time distribution.

3.5. Influence of groundwater flow on the biogeochemical Damköhler number

A characteristic residence time can be identified in the median residence time, τ_{50}, which we consider here in its dimensionless form $\tau_{50}^* = \tau_{50}\, u_m\, \lambda$. Figure 9a shows that τ_{50}^*, is constant with s^* under neutral, as long as $d_b \geq L$, losing and gaining conditions (Figure 9a). This is in contrast with the behavior of τ_m^*, which in the neutral case declines as s^* increases. A possible explanation of this differentiated behavior of τ_m^* and τ_{50}^* is that the latter is less affected than the former by the tail of the distribution [35]. The simulated median value for the neutral case is the largest and coincides with the expression obtained by Elliott and Brooks [19]. Furthermore, τ_{50}^* decreases with increasing basal velocity for both gaining and losing cases. However, slightly higher τ_{50}^* are observed under gaining than losing conditions. The difference of τ_{50}^* between gaining and losing conditions increases with v_{gw} because gaining scenarios show smaller hyporheic downwelling fluxes (Figure 6a) but same hyporheic depths (Figure 5a) than the losing conditions, thereby leading to a larger median residence time, while the mean residence time is only slightly larger (see Figures 9a and 8a).

Inspection of Figures 9a and 9b reveals that while τ_{50}^* scales with s^*, τ_{lim}^* does not, because it converges to zero as h_b^* grows large. The different behavior of these two quantities supports the choice of the two alternative scales, s^* and h_b^* in Section 2.3.

Figure 10 shows the behavior of the Damköhler number as a function of the dimensionless head h_b^* for two values of v_{gw}^*. As v_{gw}^* increases the dimension of the hyporheic cell reduces and in turn τ_{50}^* increases, thereby increasing the probability of observing prevailing aerobic conditions, which occurs for $Da_0 < 1$. Conversely, the probability to observe prevailing anaerobic conditions increases within the dimension of the hyporheic cell, as the dimensionless head increases (h_b^*) and is well represented by the following power law expression both under neutral and under gaining/losing conditions:

$$Da_O = 22901(h_b^*)^{3.357}\,,\; R^2 = 0.99 \tag{25}$$

As shown by the value of R^2 this expression explains 99% of the observed variability. This analysis provides an effective and simple method to determine the redox conditions of stream reaches with dune-like bedforms in all conceivable morphological and hydrological conditions. In equation (25), we use reach-averaged easy to evaluate morphological (H_b and L) and hydraulic (Y_0 and V) quantities without resorting to numerical simulations. Recent research has shown a correlation between Da_O and nitrogen processes, such as this analysis may provide a tool for upscaling local hyporheic processes to nitrogen cycling at the reach and network scales [38, 78, 10]. Potential weakness of our analysis are in the lack of capturing the effect of heterogeneity on removal of reactive nitrogen and the inability to differentiate mixing processes occurring in gaining from those occurring in losing conditions [29, 54]. In the former case our solutions allow to capture the average behavior of the redox conditions within the hyporheic zone from hydro-morphological and biogeochemical parameters easily measurable in the field [41]. Both under gaining and losing conditions, mixing is mostly between hyporheic cells and recharging groundwater and Da_O is similar under the same rates of groundwater downwelling and upwelling because of similar hyporheic residence times. In losing conditions, oxygenated water from the stream envelops hyporheic cells, whereas anoxic groundwater from below flows between hyporheic flow cells in gaining conditions. In a gaining stream, mixing occurring between hyporheic and ground waters reduces the concentration of dissolved oxygen in the hyporheic cells, leading to a tendency to develop more anaerobic conditions with respect to losing streams, for which the emergence of anaerobic conditions depends chiefly on the residence time of stream water within the hyporheic cells. This effect can be partially estimated with the thickness of the mixing layer.

4. Conclusions

We propose an analytical model to analyze the effects of groundwater flow on hyporheic zone hydrodynamics. Our analytical solutions encapsulate the interplay between surface hydromorphology, ambient groundwater flow (both horizontal, underflow, and vertical, basal, velocity component) on hyporheic fluxes and on the vertical extension of the hyporheic zone, defined as the zone of the alluvium receiving stream water.

We analytically identify the hyporheic flow stagnation points, which are the points where the seepage velocity is zero, and from which depart the lines defining the interface between hyporheic and ground waters, under neutral, gaining and losing conditions. ~~The effect of groundwater underflow, which is driven by a uniform head gradient equal to the streambed slope.~~[REV] It is through this interface that biogeochemical and thermal exchange occurs between shallow (i.e., hyporheic zone) and deep ground waters [31]. Thus this separation surface defines also a mixing zone and here we provide a methodology to delineate and quantify this mixing zone as well as the volume of the hyporheic zone[REV]. ~~Consequently, the hyporheic zone definition as a mixing volume between stream and ground waters should be redefined as suggested by Hester et al. [31], and we provide here a methodology to delineate and quantify the volume of the hyporheic zone.~~[REV] The proposed~~These~~[REV] analytical solutions are useful tools because they can be used (1) for testing complicated numerical models, (2) for defining a relationship between processes and governing variables (3) for identifying the governing variables in complex processes and (4) for quantifying physical quantities used to upscale hyporheic processes from the bed-form to watershed scale without the need to run complex numerical modeling [25, 41].

The location and shape of the separation surface depends on the hydromorphodynamics that controls bedform formation and the parameters that characterize groundwater flow. Consequently, from reach-scale information on the stream flow (mean flow and depth), bedform characteristics (amplitude and wavelength) and ambient groundwater velocity (basal and underflow fluxes) our solutions allow quantifying four important quantities: the hyporheic fluxes, the residence time distribution, the hyporheic vertical extension and the mean thickness of the mixing layer between hyporheic and groundwater. Redox conditions of the hyporheic flow at the reach scale can be obtained coupling these data with biogeochemical rates of dissolved oxygen consumption through the biochemical Damköhler number, Da_O, which is the ratio between hyporheic median residence time and the time limit for dissolved oxygen consumption.

Similarly to the neutral case, the hyporheic residence time is well approximated by a lognormal distribution, whose moments, i.e. mean, variance and median, assume the same values under both gaining and losing conditions with same basal velocity. Underflow affects the mean and variance but not the median of the hyporheic residence times for neutral conditions or for weak basal velocity, i.e., $v^*_{gw} < 0.1$. The stronger the underflow the smaller the upstream-flux cell gets, which eventually is suppressed when the gradient of the underflow is equal to $s_{lim} = h_m \lambda$.

Two new dimensionless length scales, s^* and h^*_b, which account for underflow flux and dune aspect ratio, respectively, facilitate the interpretation of hyporheic processes under dune-like bedform. The second is useful to understand the relationship between Da_O and reach hydromorphology. A single power law curve representing Da_O as a function of h^*_b is obtained from regression with the results of the numerical experiments, regardless the quite large differences in groundwater flow, surface hydraulics and dune shape.

List of Symbols

$\mathrm{Da_O}$	biogeochemical Damköhler number.
d_b	alluvium depth, m.
d_{50}	mean grain size, m.
DO_0	dissolved oxygen concentration, mg/l.
$DO_{0,lim}$	dissolved oxygen concentration limit, mg/l.
D_m	molecular diffusion coefficient, $\mathrm{m^2/s}$.
D_t	transverse dispersion coefficient, $\mathrm{m^2/s}$.
g	gravitational acceleration, $\mathrm{m\,s^{-2}}$.
h	hydraulic head, m.
h_m	amplitude of the dynamic head fluctuations at the bed surface, m.
h^*_b	dimensionless head.
H_d	bed form height, m.
K	hydraulic conductivity, m/s.
K_{RN}	reaction rate of nitrification and respiration, 1/s.
L	dune length, m.
n	Manning's n coefficient.
NP	number of released particles.

$\overline{q}_{H,G}$	mean groundwater flux under gaining condition, m/s.
$\overline{q}^*_{H,G}$	mean dimensionless groundwater flux under gaining condition.
$\overline{q}_{H,L}$	mean groundwater flux under losing condition, m/s.
$\overline{q}^*_{H,L}$	mean dimensionless groundwater flux under losing condition.
Q	stream discharge, m^3/s.
s	streambed slope.
s_{lim}	slope of the underflow that suppress the up-stream flux cell.
s^*	dimensionless head gradient.
T	temperature, °C.
$t_{HZ,Lmax}$	residence time along the longest hyporheic streamline, s.
$\mathbf{u} = (u, v)$	seepage velocity, m/s.
u	longitudinal pore water Darcy velocity, m/s.
u_m	maximum downwelling velocity for the neutral case, m/s.
u_0	pore water Darcy velocity scale for an infinite hyporheic zone depth, m/s.
u_s	underflow seepage velocity due to the stream slope, m/s.
V	mean stream velocity, m/s.
$\overline{u}_{HZ,Lmax}$	mean velocity along the longest hyporheic streamline, m/s.
v	vertical pore water Darcy velocity, m/s.
v_{gw}	groundwater vertical velocity, m/s.
v^*_{gw}	dimensionless vertical groundwater velocity.
$v(x, y)_{max}$	maximum value of the vertical velocity component under neutral conditions, m/s
x	longitudinal coordinate, m.
x_l	longitudinal coordinate of the stagnation point under losing condition, m.
x_g	longitudinal coordinate of the stagnation point under gaining condition, m.
y	vertical coordinate, m.
y_s	vertical position of the stagnation point under gaining and losing conditions, m.
$y_{HZ,min}$	vertical position of the deepest hyporheic point, m.
Y_0	mean flow depth, m.
$y^*_{HZ,min}$	dimensionless vertical position of the deepest hyporheic point.
y^*_s	dimensionless depth of the stagnation point under gaining and losing conditions.
Y^*	dimensionless depth equal to Y_0/H_d.
α_t	transverse dispersivity, m.
δ_{mix}	is the thickness of the mixing layer, m.
λ	dune wavenumber, m^{-1}.
μ_z	mean of the lognormal random variable, s.
σ^2	variance of the travel time, s^2.
σ^2_z	variance of the lognormal random variable, s^2.

σ^{*2}	dimensionless variance of the travel time.
ς	dune height coefficient.
τ	residence time, s.
τ_{50}	median hyporheic residence time, s.
τ_m	mean hyporheic residence time, s.
τ_{lim}	residence time limit, s.
τ^*_{50}	dimensionless median hyporheic residence time.
τ^*_{lim}	dimensionless residence time limit.
τ^*_m	dimensionless mean hyporheic residence time.
$\psi(x, y)$	stream function, m^2 s.

5. acknowledgments

This research is partially supported by the Deadwood River Project, US Forest Service Award 009421-01, by the National Science Foundation Award 1141690 and by the Italian Ministry of Public Instruction, University and Research through the project PRIN 2010-2011, prot. 2010JHF437: "Innovative methods for water resources management under hydro-climatic uncertainty scenarios". Any opinions, conclusions, or recommendations expressed in this material are those of the authors and do not necessarily reflect the views of the supporting agencies.

6. References

References

[1] Allan, J. D., Castillo, M. M., 2007. Stream Ecology. Springer, Dortrecht, The Netherlands.

[2] Alonso, C. V., Theurer, F. D., Zachmann, D. W., 1988. Tucannon river offsite study: sediment intrusion and dissolved-oxygen transport model. Tech. rep., U.S. Dept. of Agri., Agri. Res. Serv., Hydro-Ecosystem Res. Grp.

[3] Bear, J., 1972. Dynamics of fluid in porous media. Elsevier, New York.

[4] Bear, J., 1979. Hydraulics of Groundwater. McGraw-Hill, New York.

[5] Bernhardt, E. S., Hall, R. O., Likens, G. E., 2002. Whole-system estimates of nitrification and nitrate uptake in streams of the Hubbard Brook Experimental Forest. Ecosystems 5, 419–430.

[6] Boano, F., Harvey, J. W., Marion, A., Packman, A. I., Revelli, R., Ridolfi, L., Wrman, A., 2014. Hyporheic flow and transport processes: Mechanisms, models, and biogeochemical implications. Reviews of Geophysics.

[7] Boano, F., Revelli, R., Ridolfi, L., 2008. Reduction of the hyporheic zone volume due to the stream-aquifer interaction. Geophysical Research Letters 35(9), L09401.

[8] Boano, F., Revelli, R., Ridolfi, L., 2009. Quantifying the impact of groundwater discharge on the surface-subsurface exchange. Hydrol. Proc. 23, 2108–2116.

[9] Boano, F., Revelli, R., Ridolfi, L., 2010. A linear model for the coupled surface-subsurface flow in a meandering stream. Water Resour. Res. 46, W07535, doi:10.1029/2008WR007583.

[10] Briggs, M. A., Lautz, L., Hare, D. K., 2013. Residence time control on hot moments on net nitrate and uptake in hyporheic zone. Hydrol. Proc. 28, 3741–3751.

[11] Cardenas, M. B., 2009. Stream-aquifer interactions and hyporheic exchange in gaining and losing sinuous streams. Water Resour. Res 45, W06429, doi:10.1029/2008WR007651.

[12] Cardenas, M. B., Wilson, J. L., 2006. The influence of ambient groundwater discharge on exchange zones induced by current-bedform interactions. Journal of Hydrology 331, 103–109.

[13] Cardenas, M. B., Wilson, J. L., 2007. Effects of current-bed form induced fluid flow on thermal regime of sediments. Water Resour. Res 43, W08431, doi:10.1029/2006WR005343.

[14] Cardenas, M. B., Wilson, J. L., 2007. Exchange across sediment-water interface with ambient groundwater discharge. J. Hydrol. 346, 69–80.

[15] Cardenas, M. B., Wilson, J. L., Haggerty, R., 2008. Residence time of bedform-driven hyporheic exchange. Advances in Water Resources 31(10), 1382–1386.

[16] Cirpka, O. A., de Barros, F. P. J., Chiogna, G., Rolle, M., Nowak, W., 2011. Stochastic flux-related analysis on transverse mixing in two dimensional heterogeneous porous media. Water Resour. Res. 47, W06515.

[17] Dagan, G., 1989. Flow and Transport in Porous Formations. Springer-Verlag, New York.

[18] Edwards, R. T., 1998. The hyporheic zone. In: Naiman, R., Bilby, R. (Eds.), River Ecology and Management. Springer, pp. 399–429.

[19] Elliott, A. H., Brooks, N. H., 1997a. Transfer of nonsorbing solutes to a streambed with bedforms: Theory. Water Resour. Res. 33, 123–136.

[20] Elliott, A. H., Brooks, N. H., 1997b. Transfer of nonsorbing solutes to a streambed with bedforms: Laboratory experiments. Water Resour. Res. 33, 137–151.

[21] Fetter, C. W., 1994. Applied Hydrogeology. McMillian College Publishing, New York.

[22] Fogler, H. S., 1999. Elements of Chemical Reaction Engineering. Englewood Cliffs, N.J.: Prentice-Hall.

[23] Fox, A., Boano, F., Arnon, S., 2014. Impact of losing and gaining stream flow conditions on hyporheic exchange fluxes induced by dune-shaped bedforms. Water Resour. Res. 50, 1895–1907.

[24] Freeze, A. R., Cherry, J. A., 1979. Groundwater. Englewood Cliffs, N.J.: Prentice-Hall.

[25] Gomez-Velez, J. D., Harvey, J. W., 2014. A hydrogeomorphic river network model predicts where and why hyporheic exchange is important in large basins. Geophys. Res. Lett. 41, 6403–6412, doi:10.1002/2014GL061099.

[26] Gooseff, M., Anderson, J., Wondzell, S., LaNier, J., Haggerty, R., 2006. A modelling study of hyporheic exchange pattern and the sequence, size, and spacing of stream bedforms in mountain stream networks, Oregon, USA. Hydrol. Proc. 20(11), 2443–2457.

[27] Gooseff, M., Hall, R., Tank, J., 2007. Relating transient storage to channel complexity in streams of varying land use in Jackson Hole, Wyoming. Water Resour. Res. 43, W01417.

[28] Gooseff, M. N., 2010. Defining hyporheic zones: Advancing our conceptual and operational definitions of where stream water and groundwater meet. Geography Compass 4 (8), 945–955.

[29] Green, C. T., Böhlke, J. K., Bekins, B. A., Phillips, S. P., 2010. Mixing effects on apparent reaction rates and isotope fractionation during denitrification in a heterogeneous aquifer. Water Resour. Res. 46, W08525, doi:10.1029/2009WR008903.

[30] Harvey, J. W., Bhlke, J. K., Voytek, Mary, A., Scott, D., Tobias, C. R., 2013. Hyporheic zone denitrification: Controls on effective reaction depth and contribution to whole-stream mass balance. Water Resources Research 49 (10).

[31] Hester, E. T., Young, K. I., Widdowson, M. A., 2013. Mixing of surface and groundwater induced by riverbed dunes: Implications for hyporheic zone definitions and pollutant reactions. Water Resour. Res. 49, 5221–5237.

[32] Javandel, I., Tsang, C. F., 1986. Capture-zone types curves: a tool for aquifer cleanup. Ground Water 24(5), 616–625.

[33] Jiang, X. W., Wang, X. S., Wan, L., Ge, S., 2011. An analytical study of the stagnant points in the nested flow systems in basins with depth-decaying hydraulic conductivity and porosity. Water Resour. Res. 47, W01512, doi:10.1029/2010WR009346.

[34] Julien, P. Y., Klaassen, G. J., 1995. Sand dune geometry of large rivers during floods. J. Hydraul. Eng. 9(121), 657–663.

[35] Kirk, R. E., 2008. Statistics: An introduction. Thomson Higher Education, Belmont, Ca.

[36] Marion, A., Packman, A. I., Zaramella, M., Bottacin-Busolin, A., 2008. Hyporheic flows in stratified beds. Water Resour. Res. 44, W09433, doi:10.1029/2007WR006079.

[37] Marzadri, A., Tonina, D., Bellin, A., 2011. A semianalytical three-dimensional process-based model for hyporheic nitrogen dynamics in gravel bed rivers. Water Resour. Res. 47, doi:10.1029/2011WR010583.

[38] Marzadri, A., Tonina, D., Bellin, A., 2012. Morphodynamic controls on redox conditions and on nitrogen dynamics within the hyporheic zone: Application to gravel bed rivers with alternate-bar morphology. Global Biogeochem. Cycles 117, doi:10.1029/2012GJ001966.

[39] Marzadri, A., Tonina, D., Bellin, A., 2013. Effects of stream morphodynamics on hyporheic zone thermal regime. Water Resour. Res. 49, doi:10.1002/wrcr.20199.

[40] Marzadri, A., Tonina, D., Bellin, A., 2013. Quantifying the importance of daily stream water temperature fluctuations on the hyporheic thermal regime: implication for dissolved oxygen dynamics. J. Hydrol. 507, 241–248.

[41] Marzadri, A., Tonina, D., Bellin, A., Tank, J. L., 2014. A hydrologic model demonstrates nitrous oxide emissions depend on streambed morphology. Geophys. Res. Lett. 41, 54845491, doi:10.1002/2014GL060732.

[42] Marzadri, A., Tonina, D., Bellin, A., Vignoli, G., Tubino, M., 2010. Semi-analytical analysis of hyporheic flow induced by alternate bars. Water Resour. Res. 46, doi:10.1029/2009WR008285.

[43] Marzadri, A., Tonina, D., McKean, J. A., Tiedermann, M. G., Benjankar, R. M., 2014. Multi-scale streambed topographic and discharge effects on hyporheic exchange at the stream network scale in confined streams. J. Hydrol. 519(B), 1997–2011.

[44] Nield, S. P., Townley, L. R., Barr, A. D., 1994. A framework for quantitative analysis of surfacewater-groundwater interaction: Flow geometry in a vertical section. Water Resour. Res. 30, 2461–2475.

[45] Packman, A. I., Brooks, N. H., Morgan, J. J., 2000. A physicochemical model for colloid exchange between a stream and a sand streambed with bed forms. Water Resour. Res. 36(8), 2351–2361.

[46] Ren, J., Packman, A. I., 2002. Effects of background water composition on stream?subsurface exchange of submicron colloids. Journal of Environmental Engineering 128 (7), 624–634.

[47] Ren, J., Packman, A. I., 2004. Coupled stream-subsurface exchange of colloidal hematite and dissolved zinc, copper and phosphate. Environmental Science and Technology 39 (17), 6387–6394.

[48] Ren, J., Packman, A. I., 2007. Changes in fine sediment size distributions due to interactions with streambed sediments. Sedimentary Geology 202, 529–537.

[49] Rosamond, M. S., Thuss, S. J., Schiff, S. L., 2012. Dependence on riverine nitrous oxide emissions on dissolved oxygen levels. Nat. Geosci. 5, 715–718.

[50] Rubin, Y., 2003. Applied Stochastic Hydrogeology. Oxford University Press, New York.

[51] Rutherford, J. C., 1994. River Mixing. John Wiley and Sons, Chichester, England.

[52] Salamon, P., Fernàndez-Garcia, D., Gòmez-Hernàndez, J. J., 2006. A review and numerical assessment of the random walk particle tracking method. J. Contam. Hydrol. 87(3-4), 277305.

[53] Savant, A. S., Reible, D. D., Thibodeaux, R. J., 1987. Convective transport within stable river sediments. Water Resour. Res. 23, 1763–1768.

[54] Sawyer, A. H., 2015. Enhanced removal of groundwater-borne nitrate in heterogeneous aquatic sediments. Geophys. Res. Lett 42, doi:10.1002/2014GL062234.

[55] Shen, H. V., Fehlman, H. M., Mendoza, C., 1990. Bed form resistances in open channel flows. J. Hydr. Engrg. 116 (6), 799–815.

[56] Sjodin, A. L., Jr., W. M. L., III, J. F. S., 1997. Denitrification as a component of the nitrogen budget for a large plains river. Biogeochemistry 39, 327–342.

[57] Stonedahl, S. H., Harvey, J. W., Wörman, A., Salehin, M., Packman, A. I., 2010. A multiscale model for integrating hyporheic exchange from ripples to meanders. Water Resour. Res. 46, doi:10.1029/2009WR008865.

[58] Thibodeaux, L., Boyle, J. D., 1987. Bedform-generated convective-transport in bottom sediments. Nature 325(6102), 341–343.

[59] Tonina, D., 2012. Surface water and streambed sediment interaction: The hyporheic exchange. In: Habersack, H., Pigay, H., Rinaldi, M. (Eds.), Fluid mechanics of environmental interfaces. CRC Press, Taylor and Francis Group, London, UK, pp. 255–294.

[60] Tonina, D., Bellin, A., 2008. Effects of pore-scale dispersion, degree of heterogeneity, sampling size, and source volume on the concentration moments of conservative solutes in heterogeneous formations. Adv. Water Resour. 31(2), 339–354.

[61] Tonina, D., Buffington, J. M., 2007. Hyporheic exchange in gravel bed rivers with pool-riffle morphology: laboratory experiment and three-dimensional modeling. Water Resour. Res. 43, 1–16.

[62] Tonina, D., Buffington, J. M., 2009. Hyporheic exchange in mountain rivers I: Mechanics and environmental effects. Geography Compass 3(3), 1063–1086.

[63] Tonina, D., Buffington, J. M., 2009. A three-dimensional model for analyzing the effects of salmon redds on hyporheic exchange and egg pocket habitat. Canadian Journal of Fisheries and Aquatic Sciences 66, 2157–2173.

[64] Tonina, D., Buffington, J. M., 2011. Effects of stream discharge, alluvial depth and bar amplitude on hyporheic flow in pool-riffle channels. Water Resour. Res. 47, doi:10.1029/2010WR009140.

[65] Tonina, D., Marzadri, A., Bellin, A., 2015. Benthic uptake rate due to hyporheic exchange: The effects of streambed morphology for constant and sinusoidally varying nutrient loads. Water 7, 398–419, doi:10.3390/w7020398.

[66] Tonina, D., McKean, J. A., Tang, C., Goodwin, P., 2011. New tools for aquatic habitat modeling. Proceedings of the 34th IAHR World Congress 2011, Brisbane, Australia, pp. 3137–3144.

[67] Tóth, J., 1963. A theorethical analysis of groundwater flow in small drainage basins. J. Geophys. Res. 68, 4795–4812.

[68] Trauth, N., Schimdt, C., Maier, U., Vieweg, M., Fleckenstein, J. H., 2013. Coupled 3d stream flow and hyporheic flow model under varying stream and ambient groundwater flow conditions in pool-riffle system. Water Resour. Res. 49 (5834-5850).

[69] Triska, F. K., Duff, J. H., Avanzino, R. J., 1993. The role of water exchange between a stream channel and its hyporheic zone in nitrogen cycling at the terrestrial-aquatic interface. Hydrobiologia 251, 167–184.

[70] Vaux, W. G., 1968. Intragravel flow and interchange of water in a streambed. Fish. Bull. 66(3), 479–489.

[71] Vittal, N., Raju, K. R., Garde, R., 1977. Resistance of two-dimensional triangular roughness. J. Hydraul. Res. 15(1), 19–36.

[72] Werth, C. J., Cirpka, O. A., Grathwohl, P., 2006. Enhanced mixing and reaction through flow focusing in heterogeneous porous media. Water Resour. Res. 42, W12414, doi:10.1029/2005WR004511.

[73] Winter, T. C., 1999. Relation of streams, lakes, and wetlands to groundwater flow systems. Hydrogeol J. 7(1), 1–14.

[74] Winter, T. C., Pfannkuch, H. O., 1976. Hydrogeology of a drift-filled bedrock valley near Lino Lakes, Anoka County, Minnesota. US Geol. Surv. J. Res. 4(3), 267–276.

[75] Wörman, A., Packman, A. I., Johansson, H., Jonsson, K., 2002. Effect of flow-induced exchange in hyporheic zones on longitudinal transport of solutes in stream and rivers. Water Resour. Res. 38, 2–15.

[76] Yalin, M. S., 1964. Geometrical properties of sand waves. J. Hydraul. Div., Am. Soc. Civ. Eng. 90(5), 105–119.

[77] Zarnetske, J. P., Haggerty, R., Wondzell, S. M., Baker, M. A., 2011. Dynamics of nitrate production and removal as a function of residence time in the hyporheic zone. J. Geophys. Res. 116, doi:10.1029/2010JG001356.

[78] Zarnetske, J. P., Haggerty, R., Wondzell, S. M., Bokil, V. A., González-Pinzón, R., 2012. Coupled transport and reaction kinetics control on the nitrate sources-sink function of hyporheic zones. Water Resour. Res. 48(11), doi:10.1029/2012WR011894.

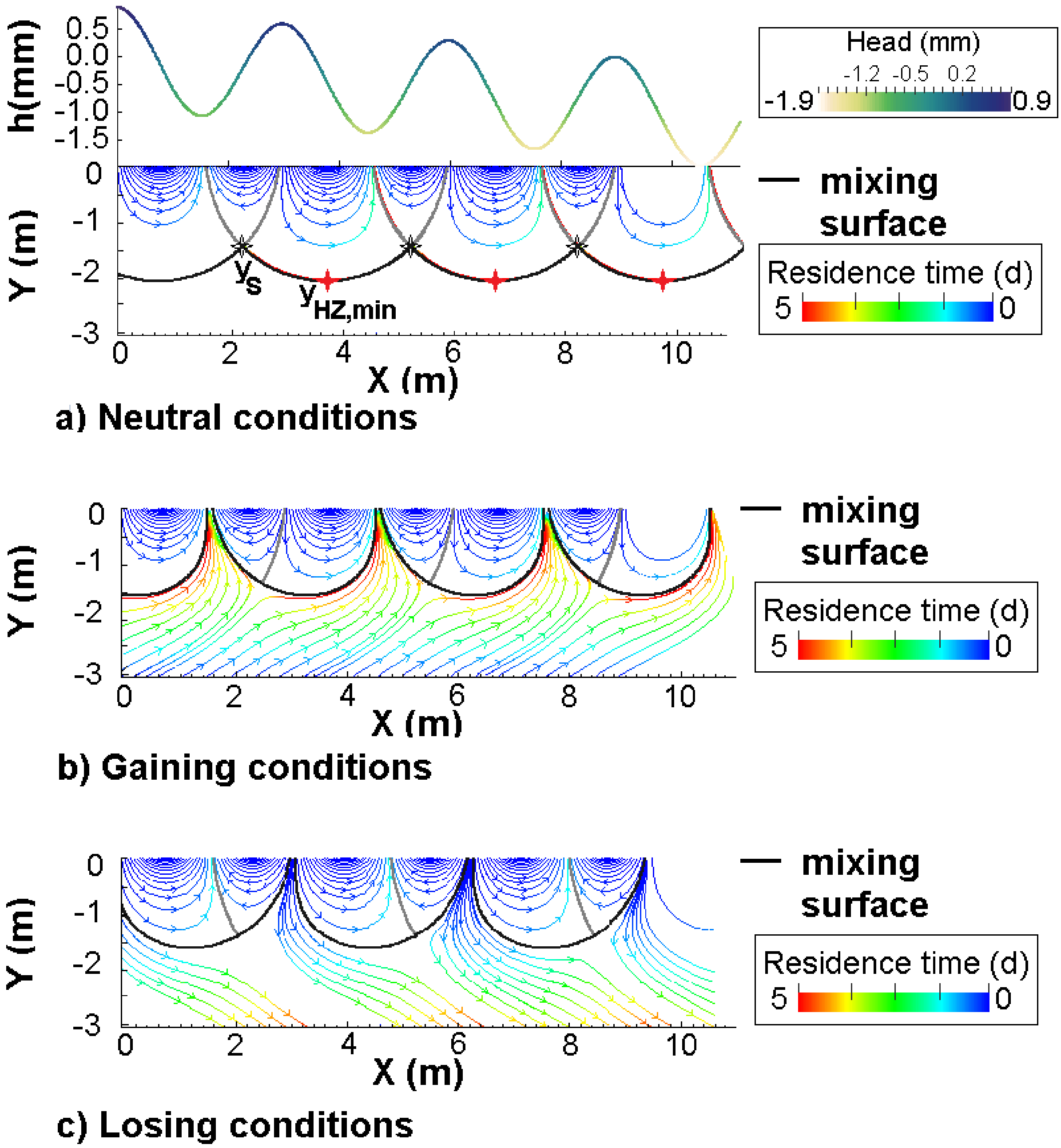

Figure 2: Analytical flow field under (a) neutral, (b) gaining and (c) losing conditions for Test 30 (Table S1 in Supplementary Information). The positions of both the minimum streamline depth $y_{HZ,min}$ and the stagnant points y_s are showed for the neutral case. The energy head distribution at the water-sediment interface showed in subfigure (a) is valid also under gaining and losing conditions.

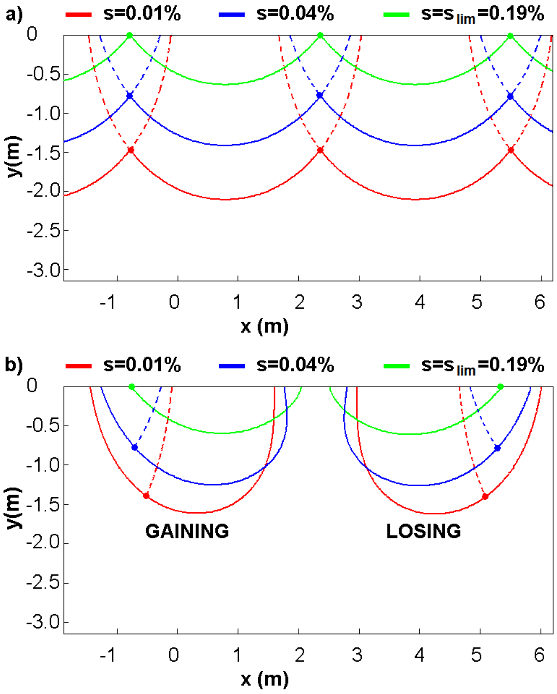

Figure 3: Stream functions ψ tracing the separation between the hyporheic cells and the surrounding groundwater environment (solid lines) and between conterminous hyporheic flow cells (dashed lines) for the following three stream slopes: $s = 0.01\%$, $s = 0.04\%$ and $s = s_{lim} = 0.19\%$ under (a) neutral and (b) gaining and losing conditions. The stream functions are obtained with the morphodynamic parameters of Test 30 in Table S1 (Supplementary Information) with the following Manning's coefficients: $n = 0.0125$ when $s = 0.01\%$, $n = 0.025$ when $s = 0.04\%$ and $n = 0.054$ when $s = s_{lim} = 0.19\%$ and a dune length $L = 3m$. The stagnation points are marked with filled circles.

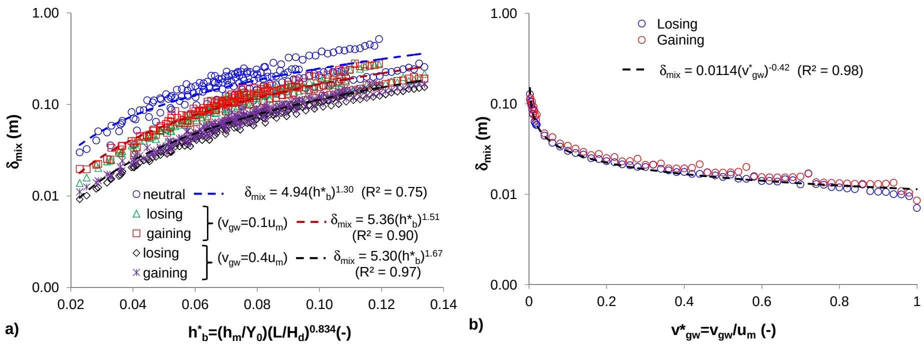

Figure 4: Trend of variation of the thickness of the mixing layer δ_{mix} as a functions of (a) the dimensionless head h_b^* and (b) the dimensionless basal velocity v_{gw}^*.

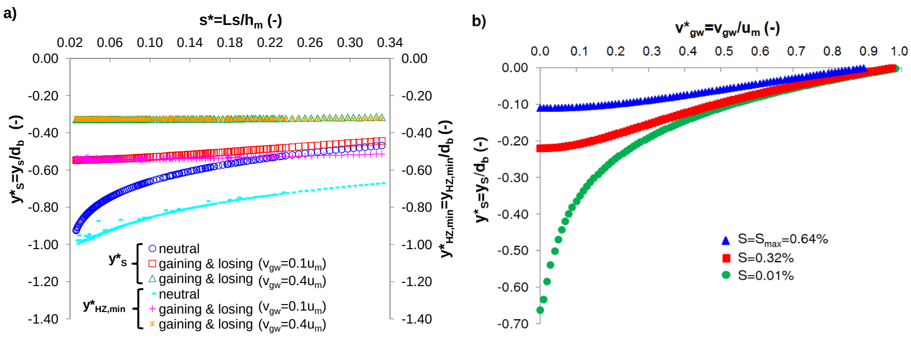

Figure 5: (a) Positions of the stagnation point, y_s^* (analytical solution), and of the deepest point of the hyporheic cell, $y_{HZ,min}^*$ (numerical solution), as a function of the dune dimensionless energy gradient s^* under different gaining and losing conditions. Comparison with neutral case is also showed; and (b) Position of the stagnation point y_s^* as a function of the dimensionless groundwater velocity (gaining and losing) v_{gw}^* for Test120 in Table S4 of the Supplementary Information with the following Manning's coefficients: $n = 0.0125$ for $s = 0.01\%$, $n = 0.071$ for $s = 0.32\%$ and $n = 0.1$ for $s = s_{lim} = 0.64\%$.

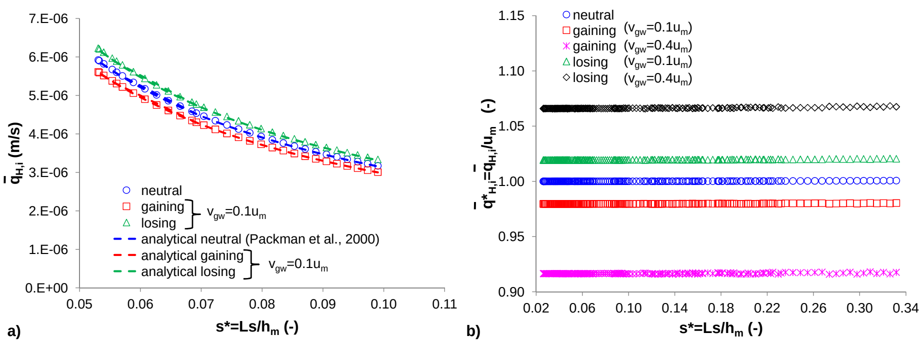

Figure 6: (a) Trend of variation of the hyporheic downwelling fluxes (analytical solution in dashed lines and numerical solution with symbols), $\overline{q}_{H,i}$ ($i = G$ and $i = L$ under gaining and losing conditions, respectively) as a function of the dimensionless energy gradient s^* for dunes with $H_d/L = 0.04$ (whose morphodynamics parameters are reported in Table S4 of the Supplementary Information). (b) Trend of variation of the dimensionless hyporheic downwelling fluxes $\overline{q}_{H,i}^* = \overline{q}_{H,i}/u_m$ under different gaining ($i = G$) and losing ($i = L$) conditions as a function of the dimensionless energy gradient s^*.

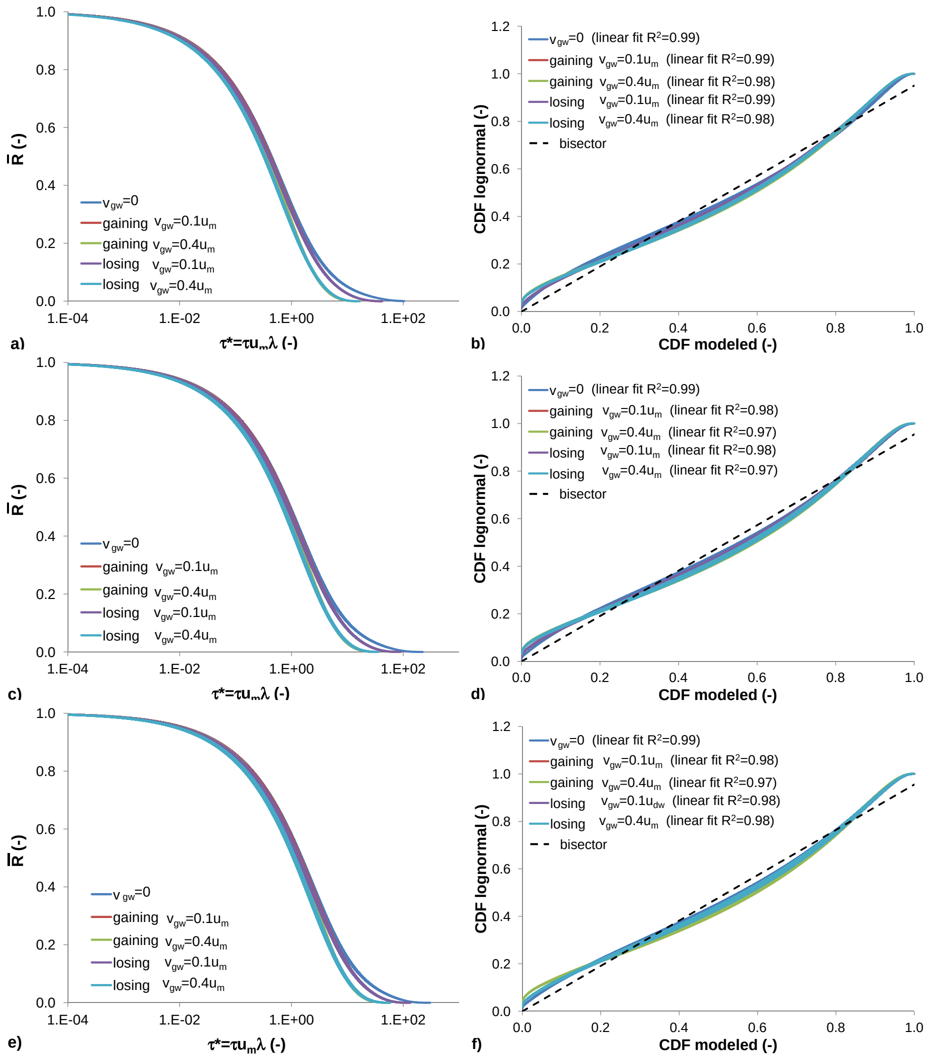

Figure 7: Exceedance probability of the hyporheic residence time distribution for the morphological parameters of: (a) Test 95, (c) Test 105 and (e) Test 115 in Table S4 under different gaining or losing conditions. The sample CDF is compared with the Log-Normal distribution for the following cases: (b) Test 95, (d) Test 105 and (f) Test 115 in Table S4 under different gaining and losing conditions.

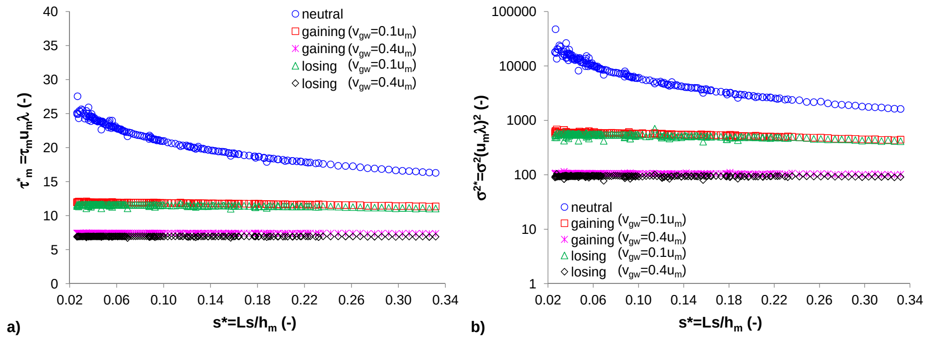

Figure 8: Mean, τ_m^*, (a) and variance, σ^{*2}_{τ}, (b) of the dimensionless residence time τ^* as a function of the dimensionless energy gradient s^*.

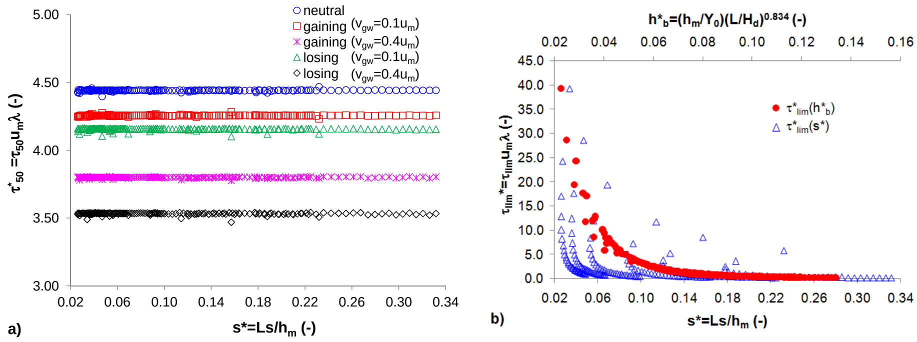

Figure 9: (a) Median of the dimensionless residence time τ_{50}^* as a function of the dimensionless energy gradient s^*. (b) Dimensionless residence time limit τ_{lim} as a function of the dimensionless energy gradient s^* and the dimensionless head h_b^*.

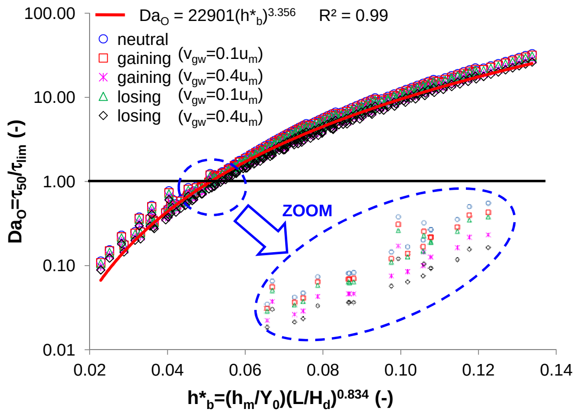

Figure 10: Trend of variation of the biogeochemical Damköhler number Da_O as a function of the dimensionless head h_b^*.